

Article

Reflection Enhancement and Giant Lateral Shift in Defective Photonic Crystals with Graphene

Dong Zhao †, Fangmei Liu †, Peng Meng *, Jie Wen, Siliu Xu, Zhongming Li and Dong Zhong *

School of Electronic and Information Engineering, Hubei University of Science and Technology, Xianning 437100, China; zhaodong@hbust.edu.cn (D.Z.); liufangmei@hbust.edu.cn (F.L.); wenjie@hbust.edu.cn (J.W.); lizhongming@hbust.edu.cn (Z.L.)

* Correspondence: mengpeng@hbust.edu.cn (P.M.); zhongdong@hbust.edu.cn (D.Z.)

† These authors contributed equally to this work.

Received: 24 April 2019; Accepted: 14 May 2019; Published: 25 May 2019

Featured Application: highly sensitive sensor

Abstract: This study investigates the reflectance of the defective mode (DM) and the lateral shift of reflected beam in defective photonic crystals incorporated with single-layer graphene by the transfer matrix method (TMM). Graphene, treated as an equivalent dielectric with a thickness of 0.34 nm, was embedded in the center of a defect layer. The reflectance of the DM was greatly enhanced as the intraband transition of electrons was converted to an interband transition in graphene. The reflectance of the DM could be further enhanced by increasing the Bragg periodic number. Furthermore, a large lateral shift of the reflected beam could also be induced around the DM. This study may find great applications in highly sensitive sensors.

Keywords: reflection enhancement; lateral shift; defective mode; photonic crystal; graphene

1. Introduction

It is well known that the most typical property of photonic crystals (PCs) is the photonic bandgap structure [1]. As a light beam impinges upon PCs, there is a large lateral shift of the reflected beam on the bandgap edge [2]. The shift of reflected beam, which can be spatial and angular, was firstly confirmed experimentally by Goos and Hänchen [3]. The spatial shift and angular deviation from the prediction of geometrical optics essentially result from the dispersion of reflection coefficients, and could be estimated by the famous Artmann formula [4]. Giant lateral shift has also been reported inside the reflection band, and become extremely large at exceptional points (EPs) in parity–time-symmetric (PT-symmetric) PCs [5]. Furthermore, a great lateral shift may also exist in non-Hermitian systems and periodic dielectric multilayers with PT-symmetry [6,7]. Meanwhile, low loss in slabs and defects embedded in PCs can greatly enhance the lateral shift [8,9]. The defective mode (DM) locates at the middle of the bandgap in defective PCs. The lateral shift of the reflected beam near the DM is generally dozens of incident wavelengths, and the reflectivity of the DM can be as low as zero in passive PCs. On the other hand, non-Hermitian systems can induce many unique optical phenomena, and have become a hot topic in optics and other fields [10–17]. In non-Hermitian systems, large lateral shift can be obtained near exceptional point (EP) and coherent-perfect-absorption (CPA)-laser state [5,6,18], but the reflectivity of the EP is also zero and the reflectivity is very low near it [19–21] while the CPA-laser state is unstable, so these are not conducive to the observation of lateral shift for reflected beams.

Graphene is an ultrathin two-dimensional material, and it has been studied intensively for its fascinating optical, electronic, and mechanical properties [22–26]. The surface conductivity of

graphene could be flexibly modulated by chemical doping or external gate voltages, and the low loss in graphene exists across a wide frequency range [27,28]. Therefore, we constructed a complex system composed of graphene and defective PCs, of which the surface current of graphene could be utilized to enhance the reflectance of the DM and a giant lateral shift could be induced to obtain low loss in graphene.

In this study, we investigated the enhancement of reflectance and the lateral shift of reflected beams in defective PCs incorporated with graphene. Graphene was embedded in the PCs to enhance the reflectance of the DM by utilizing the transition conversion of electrons in graphene. Subsequently, we calculated the reflection of the DM for different Bragg periodic numbers. Finally, we studied the lateral shift of reflected beams around the DM as well as the tunability of the lateral shift.

2. One-Dimensional Defective PCs

Figure 1 shows a schematic of the one-dimensional defective PCs. The dielectrics A and B were arranged alternatively on both sides of the defect layer C, forming two Bragg gratings. The defective system could also be viewed as a Fabry–Pérot resonant cavity, in which the Bragg gratings are two reflectors and the defect layer plays the role of cavity. A single-layer graphene was embedded in the center of the defect layer. The thickness of dielectrics A and B was $\lambda_0/4n$, where $\lambda_0 = 1.55 \mu\text{m}$ denotes the midgap (resonant) wavelength of the defective periodic multilayers. The thickness of the defect layer C was $\lambda_0/2n$. The refractive indices of dielectric were $n_a = 1.38$ and $n_b = n_c = 2.35$, respectively.



Figure 1. Schematic of defective photonic crystals (PCs). The primitive unit-cell layers A and B array alternatively to form two Bragg gratings. Graphene (G) is embedded in the center of the defect layer C.

Graphene is a two-dimensional material, and we treated it as an equivalent dielectric with a thickness of $d_g = 0.34 \text{ nm}$ [29,30]. The surface conductivity of graphene can be modulated by chemical doping or gate voltages, so the type of graphene can be doped or pure. Subsequently, the relative equivalent permittivity of graphene can be given by $\epsilon_g = 1 + i\sigma_g\eta_0/(kd_g)$ [28], where $k = 2\pi/\lambda$ is the wave number of incident light in vacuum, η_0 is the vacuum resistivity, and σ_g is the total surface conductivity of graphene. The parameter σ_g can be written as $\sigma_g = \sigma^{(1)} + \sigma^{(3)}|E_z|^2$, where $\sigma^{(1)}$ is the linear surface conductivity of graphene and $\sigma^{(3)}$ is the nonlinear coefficient of surface conductivity. Here we assumed that the input intensity of light was low enough and ignored the nonlinear effect of graphene. The linear surface conductivity is governed by the Kubo formula [27,31], which depends on the incident wavelength λ , chemical potential μ , absolute temperature T , and momentum relaxation time τ . We chose the incident wavelength around λ_0 , and set $\tau = 0.5 \text{ ps}$, $T = 300 \text{ K}$ in the following study. As a light beam impinges upon the system, the reflection and transmission coefficients are denoted by r and t , respectively. The two coefficients could be obtained by the transfer matrix method (TMM) [32]. The transmittance T is identified as $T = tt^* = I_t/I_i$, where I_t and I_i are the transmitted and incident intensities, respectively. The reflectance R is identified as $R = rr^*$.

3. Reflectance Enhanced with Graphene

Now we calculate the transmission and reflection spectra as the TM wave obliquely impinges upon the defective PCs incorporated without graphene. The incident angle is $\theta = 20^\circ$. Figure 2a shows the transmittance spectra for three different Bragg periodic numbers $N = 3, 4, \text{ and } 5$, respectively. The transmittance varies with the normalized frequency $(\omega - \omega_0)/\omega_{gap}$, where the photonic bandgap of PCs is $\omega_{gap} = 4\omega_0 \arcsin|(n_b - n_a)/(n_b + n_a)|^2/\pi$ [1], and $\omega_0 = 2\pi c/\lambda_0$ is the center frequency of the bandgap.

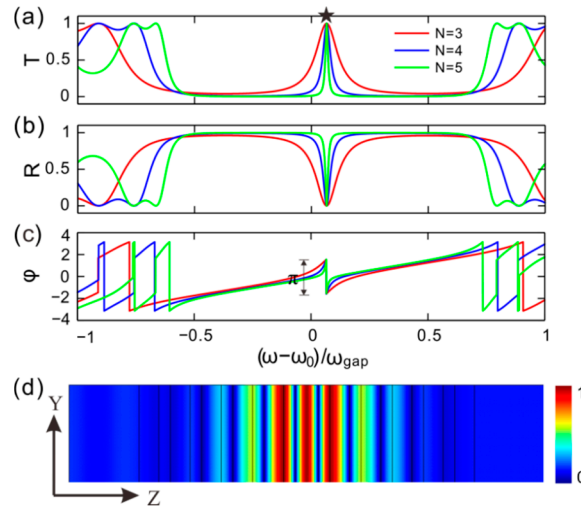


Figure 2. The calculated spectra for the defective photonic crystals (PCs) without graphene. (a) The transmission spectrum T . (b) The reflection spectrum R . (c) The phase of the reflection coefficient. (d) Electric field intensity ($|E_z|^2$) distribution of the defect mode.

There was a peak in each spectrum near the zero point of normalized frequency. The maximum value $T_m = 1$ at the spectrum center $(\omega - \omega_0)/\omega_{\text{gap}} = 0.065$ corresponds to the transmittance of the DM, denoted by a star symbol. The transmission spectrum width was smaller for a larger Bragg periodic number N , demonstrating its good frequency selectivity. Figure 2b shows the reflectance spectrum. The reflectances of the DM were all as low as zero for the three Bragg periodic numbers. This shows that there was no light reflected from the PCs, as the incident frequency identified with the DM. The PCs became transparent for this specific frequency wave, so the DM is also known as a transmission mode. Figure 2c shows the phase of the reflection coefficient. The phase varied with the normalized frequency. There was a π phase hopping at the DM in each phase curve for different Bragg periodic numbers. The reflectance was zero at the DM, which resulted in uncertainty in the phase of the reflection coefficient. Figure 2d shows the distribution of the DM. It illustrates that the electric field was mainly localized at the defect layer, and the electric field exponentially decayed as it departed from the center along the z -axis.

We embedded single-layer graphene in the middle of the defect and investigated the influence on transmittance, reflectance, and phase of the reflection coefficient with the interaction between the graphene and the electric field of the DM. Figure 3a shows the transmittance spectra. One can find that the transmittance of the DM was no longer constant, and decreased with the increase of the Bragg periodic number N . On the contrary, the reflectance of the DM increased with the Bragg periodic number, as shown in Figure 3b. In other words, the reflection intensity of light could be greatly enhanced by increasing N .

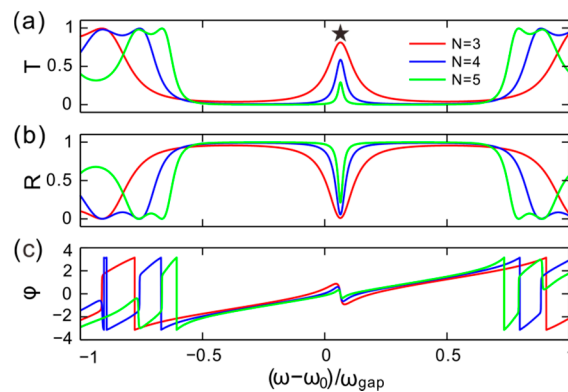


Figure 3. The calculated spectra for the defective photonic crystals (PCs) incorporated with graphene. (a) The transmission spectrum T . (b) The reflection spectrum R . (c) The phase of the reflection coefficient. The chemical potential was $\mu_c = 0.15$ eV.

The reflection coefficient is represented by $r = |r|\exp(i\varphi)$, where φ is the phase change of the reflected beam. The graphene inset at the defect therefore apparently influenced the reflection behavior of light—especially the reflection phase. Figure 3c shows that the reflection phase varied continuously with the normalized frequency, but did not change abruptly at the DM. As the frequency increased, the phase changed dramatically around the DM. This behavior indicates that a large lateral shift of the reflected beam may have been induced, since the lateral shift was proportional to the curvature of the phase curve.

The surface conductivity is a function of the chemical potential of graphene, so the optical properties can be readily modulated by the chemical potential. Figure 4a shows the transmittance of light in the parameter space composed of the normalized frequency and the chemical potential of graphene. We took the logarithm $\log_{10}R$ for increasing image contrast. One can see that the transmittance was a function of these two parameters. As the chemical potential increased, the transmittance varied with the normalized frequency. For a fixed chemical potential, there was a maximum in each transmission spectrum. The maximum corresponded to the transmittance of the DM. This demonstrates that the frequency of the DM remained approximately constant as the chemical potential changed, while the transmittance changed abruptly near $\mu_c = 0.41$ eV. The transmission mode (i.e., the DM) corresponded to the maximum of transmission spectrum in the middle of the bandgap.

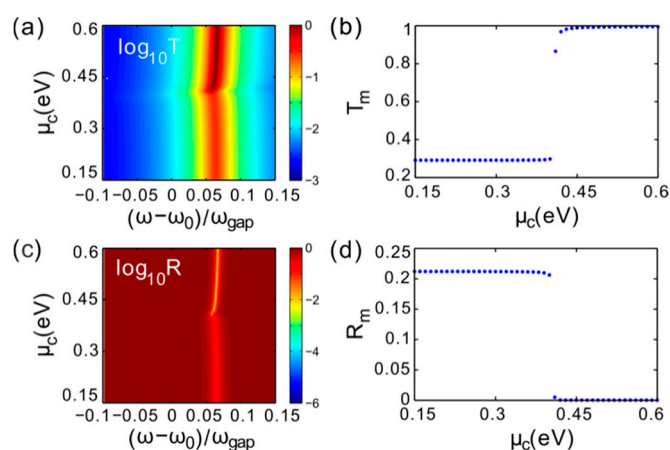


Figure 4. (a,c) The transmittance and reflectance varying with the chemical potential and normalized frequency, respectively. (b,d) The transmittance and reflectance of the defect mode. The Bragg periodic number $N = 5$.

Figure 4b shows the transmittance of the DM for different chemical potential. It shows that the maximum was $T_m = 0.29$ when the chemical potential $\mu_c < 0.41$ eV, and the maximum was $T_m = 0.99$ when the chemical potential $\mu_c > 0.41$ eV. Figure 4c shows the reflectance of light. It demonstrates that the position of minimum reflectance goes along with the DM in the parameter space as the chemical potential changed. Figure 4d shows the minimum reflectance in the bandgap. It shows the maximum changed with the chemical potential of graphene. The value was $R_m = 0.21$ when the chemical potential $\mu_c < 0.41$ eV, and the minimum was $R_m = 0$ when the chemical potential $\mu_c > 0.41$ eV. The surface conductivity of graphene is contributed by electron movement. The intraband transition of electron movement governs mainly for a low chemical potential, while the interband transition plays a leading role for a high chemical potential [24,31].

Figure 5a shows the real part of the surface conductivity of graphene. It varied with the chemical potential of graphene. As $\mu_c < 0.41$ eV, the real part of the surface conductivity of graphene was close to 0.6 S. High surface conductivity corresponds to a strong surface current, which can induce reflection enhancement in the DM. The real part of the surface conductivity of graphene was close to zero as $\mu_c > 0.41$ eV, in which the graphene presented complete transparency. Figure 5b shows the imaginary part of the surface conductivity of graphene. There was a minimum in the imaginary part curve as the chemical potential changed. The imaginary part of the surface

conductivity is equivalent to the real part of the refractive index if we regard the graphene as an equivalent dielectric. Therefore, the center frequency of DM may vary with the chemical potential of graphene. Furthermore, the periodic structure of the system can also influence the reflectance of the DM, as shown in Figure 5c. The chemical potential took a fixed value of $\mu_c = 0.15$ eV. One can see that the reflectance of DM increased with the increase of the Bragg periodic number N , while the transmittance of the DM decreased. The resonance of the DM was stronger for larger N . The enhancement of the local field where the graphene was located contributed to the interband transition of electrons as the Bragg number N increased.

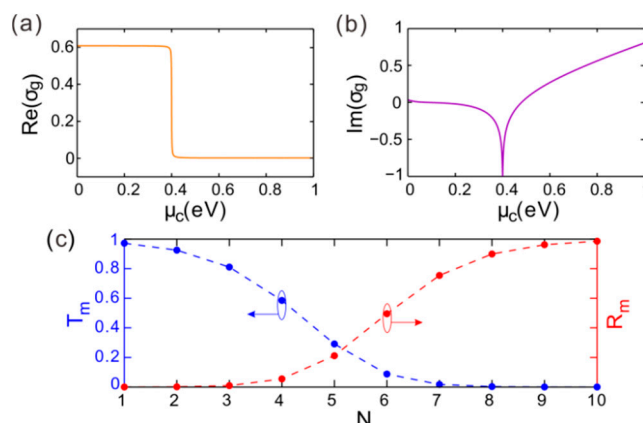


Figure 5. (a,b) The real and imaginary parts of surface conductivity of graphene, respectively. (c) The transmittance and reflectance of the defective mode (DM) varying with the Bragg periodic number N .

4. Large Lateral Shift around the DM

Figure 6a shows the phase of the reflection coefficient. For each fixed chemical potential, there is a corresponding phase curve. The phase varied with the normalized frequency. The change in phase became particularly dramatic in the area around the DM. Especially, the phase approximated a step change at the DM as the chemical potential $\mu_c > 0.41$ eV. To demonstrate the details of the phase change, Figure 6b depicts the phase curve for three different chemical potentials: $\mu_c = 0.25, 0.41,$ and 0.60 eV. One can see that the phase varied with the normalized frequency. Around the DM, the curvature was negative, but it became positive as the frequency extended to both sides beyond the DM. The interval of phase change at the DM enlarged as the chemical potential increased and the change in phase approached π ; even so, the phase curve still varied continuously and there was no hopping in phase. This means that a higher chemical potential may lead to a greater change in the phase of the reflection coefficient around the DM. The loss of graphene decreased greatly as the chemical potential exceeded 0.41 eV. Low loss in materials can induce a sharp change in the reflection coefficient phase [6].

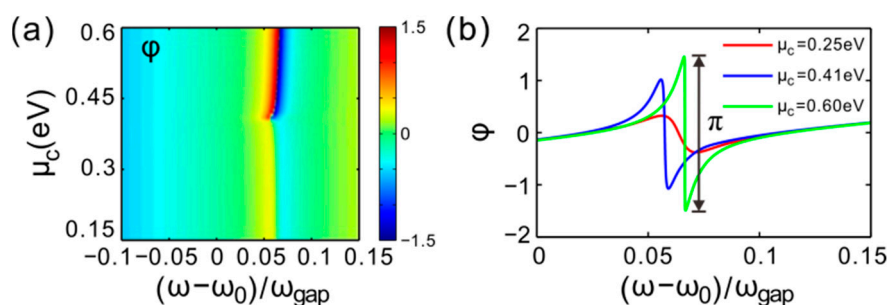


Figure 6. (a) The phase of the reflection coefficient. The parameter space composed of the chemical potential and normalized frequency. (b) The reflection coefficient phase varying with the normalized frequency. The Bragg periodic number $N = 5$.

As an incident beam impinges upon the structure, the lateral shift of the reflected beam can be derived by $\Delta = -d\varphi/dk$ [33]. Figure 7a shows the lateral shift in the parameter space composed of the chemical potential and normalized frequency. For each fixed chemical potential, the lateral shift of the reflected beam can be positive or negative as the normalized frequency changes, and the extrema are very large. Therefore, for better contrast, we took the logarithm of the absolute lateral shift (i.e., $\log_{10}|\Delta|$). One can see that the lateral shift was large in the region around the DM in the parameter space. There was an obvious difference in the lateral shift near the chemical potential $\mu_c = 0.41$ eV.

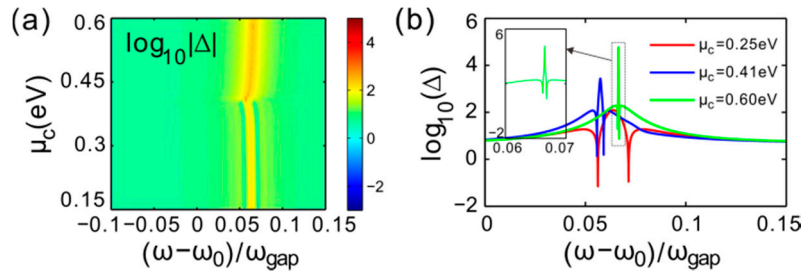


Figure 7. (a) The lateral shift of reflected beam in the parameter space. (b) The lateral shift varying with the normalized frequency. The Bragg periodic number $N = 5$.

Figure 7b shows the lateral shift of the reflected beam for different chemical potential. The lateral shift is a function of the normalized frequency. There was a peak and two valleys in each curve of lateral shift. The extrema were $\Delta = 124\lambda$, -18.8λ , and -18.9λ for $\mu_c = 0.25$ eV. The extrema were $\Delta = 2.74 \times 10^3\lambda$, -118.6λ , and -117.4λ for $\mu_c = 0.41$ eV. The extrema were $\Delta = 5.74 \times 10^4\lambda$, -118.9λ , and -119λ for $\mu_c = 0.60$ eV. Therefore, by increasing the frequency, the peak in the shift curve became sharper and the gap between the two valleys reduced. This super-sensitive lateral shift effect of reflected beam could be used for the detection of weak physical effects [34,35]. The surface conductivity of graphene is a function of the chemical potential and normalized frequency. The loss is lower for larger chemical potential. Low loss can cause violent fluctuation in phase of reflection coefficient around the DM as the normalized frequency changes, and then the dramatic fluctuation in phase induces large lateral shift of reflected beam. We only used TM waves as the typical incident beam in the present study. In fact, when TE waves were used for calculation, similar results were obtained. When the structure is fixed, the reflection spectrum is a function of incident angle and incident wavelength. Different incident angles only affect the location of the defect mode, but the reflectivity enhancement and giant lateral shift near the defect mode are not affected. Here, we selected the incident angle of 20° , which has no special meaning—it is just a typical example to illustrate our simulation results. The conductivity of multilayer graphene can be described by $\sigma_{ml} = \sigma_g N_{gra}$ as $N_{gra} < 7$, where N_{gra} is the number of graphene layers [36]. Subsequently, the relative equivalent permittivity of multilayer graphene could be given by $\epsilon_{ml} = 1 + i\sigma_{ml}\eta_0/(kN_{gra}d_g) = 1 + i\sigma_g\eta_0/(kd_g)$, which is equal to the equivalent permittivity of single-layer graphene ϵ_g . We simulated the cases of double and multilayer graphene, and results showed that the main conclusion was not affected by the number of layers.

5. Conclusions

We studied the reflectance of DM and the lateral shift of the reflected beam in defective PCs with graphene embedded in the center of the defect layer. High reflectivity of the DM and giant lateral shift near the DM were realized simultaneously. The interband transition of electrons in graphene greatly enhanced the reflection of the DM, and its reflectance could be as high as 0.21 for the Bragg periodic number $N = 5$. The reflectance could be further enhanced by increasing the number N . Meanwhile, large lateral shift of the reflected beam was induced, and the shift could be positive or negative. The maximum of lateral shift approached the magnitude of $10^4\lambda$ around the DM. The lateral shift could also be tuned by the chemical potential of graphene. This study paves the way for the development of highly sensitive sensors.

Author Contributions: software, F.L. and J.W.; investigation, D.Z. and D. Z.; writing—original draft preparation, D.Z.; writing—review and editing, D.Z., P.M., S.X. and D. Z.; funding acquisition, Z.L. and D.Z.

Funding: National Natural Science Foundation of China (NSFC) (61575148); Natural Science Foundation of Hubei Province (2015CFA040, 2016CFB515); Educational Commission of Hubei Province (D20172803); Humanities and Social Science Project of Hubei Education Department (18Q164); Colleges and Universities of National Innovation and Entrepreneurship Training Plan (201710927006Z, 201810927011).

Conflicts of Interest: The authors declare no conflicts of interest.

References

1. Yariv, A.; Yeh, P. *Photonics: Optical Electronics in Modern Communications*, 6th ed.; Oxford University Press: New York, NY, USA, 2007.
2. Felbacq, D.; Moreau, A.; Smaâli, R. Goos-Hänchen effect in the gaps of photonic crystals. *Opt. Lett.* **2003**, *28*, 1633–1635.
3. Goos, F.; Hänchen, H. A new and fundamental experiment on total reflection. *Ann. Phys.* **1947**, *1*, 333.
4. Aiello, A.; Woerdman, J.P. Role of beam propagation in Goos-Hänchen and Imbert-Fedorov shifts. *Opt. Lett.* **2008**, *33*, 1437–1439.
5. Longhi, S.; della Valle, G.; Staliunas, K. Goos-Hänchen shift in complex crystals. *Phys. Rev. A* **2011**, *84*, 042119.
6. Ma, P.; Gao, L. Large and tunable lateral shifts in one-dimensional PT-symmetric layered structures. *Opt. Express* **2017**, *25*, 9676–9688.
7. Zhao, D.; Ke, S.; Liu, Q.; Wang, B.; Lu, P. Giant Goos-Hänchen shifts in non-Hermitian dielectric multilayers incorporated with graphene. *Opt. Express* **2018**, *26*, 2817–2828.
8. Wang, L.G.; Chen, H.; Zhu, S.Y. Large negative goos-hänchen shift from a weakly absorbing dielectric slab. *Opt. Lett.* **2005**, *30*, 2936–2938.
9. Wang, L.G.; Zhu, S.Y. Giant lateral shift of a light beam at the defect mode in one-dimensional photonic crystals. *Opt. Lett.* **2006**, *31*, 101–103.
10. Ke, S.; Liu, J.; Liu, Q.; Zhao, D.; Liu, W. Strong absorption near exceptional points in plasmonic wave guide arrays. *Opt. Quant. Electron.* **2018**, *50*, 318.
11. Li, M.; Xie, H.; Cao, W.; Luo, S.; Tan, J.; Feng, Y.; Du, B.; Zhang, W.; Li, Y.; Zhang, Q.; et al. Photoelectron holographic interferometry to probe the longitudinal momentum offset at the tunnel exit. *Phys. Rev. Lett.* **2019**, *122*, 183202.
12. He, Y.; He, L.; Lan, P.; Wang, B.; Li, L.; Zhu, X.; Cao, W.; Lu, P. Molecular rotation movie filmed with high-harmonic generation. *arXiv* **2019**, arXiv:1902.05662.
13. Ke, S.; Zhao, D.; Liu, Q.; Liu, W. Adiabatic transfer of surface plasmons in non-Hermitian graphene waveguides. *Opt. Quant. Electron.* **2018**, *50*, 393.
14. Ke, S.; Zhao, D.; Liu, Q.; Wu, S.; Wang, B.; Lu, P. Optical imaginary directional couplers. *J. Lightwave Technol.* **2018**, *36*, 2510–2515.
15. Xu, S.L.; Zhao, Y.; Petrović, N.Z.; Belić, M.R. Spatiotemporal soliton supported by parity-time symmetric potential with competing nonlinearities. *EPL* **2016**, *115*, 14006.
16. Xu, S.L.; Petrović, N.; Belić, M.R.; Hu, Z.L. Light bullet supported by parity-time symmetric potential with power-law nonlinearity. *Nonlinear Dyn.* **2016**, *84*, 1877–1882.
17. Ke, S.; Zhao, D.; Liu, J.; Liu, Q.; Liao, Q.; Wang, B.; Lu, P. Topological bound modes in anti-PT-symmetric optical waveguide arrays. *Opt. Express* **2019**, *27*, 13858–13870.
18. Zhao, D.; Zhong, D.; Hu, Y.; Ke, S.; Liu, W. Imaginary modulation inducing giant spatial Goos-Hänchen shifts in one-dimensional defective photonic lattices. *Opt. Quant. Electron.* **2019**, *51*, 113.
19. Ke, S.; Wang, B.; Qin, C.; Long, H.; Wang, K.; Lu, P. Exceptional points and asymmetric mode switching in plasmonic waveguides. *J. Lightwave Technol.* **2016**, *34*, 5258–5262.
20. Zhu, X.F. Defect states and exceptional point splitting in the band gaps of one-dimensional parity-time lattices. *Opt. Express* **2015**, *23*, 22274–22284.
21. Liu, Q.; Wang, B.; Ke, S.; Long, H.; Wang, K.; Lu, P. Exceptional points in Fano-resonant graphene metamaterials. *Opt. Express* **2017**, *25*, 7203–7212.
22. Dai, X.; Jiang, L.; Xiang, Y. Tunable optical bistability of dielectric/nonlinear graphene/dielectric heterostructures. *Opt. Express* **2015**, *23*, 6497–6508.

23. Zhao, D.; Wang, Z.Q.; Long, H.; Wang, K.; Wang, B.; Lu, P.X. Optical bistability in defective photonic multilayers doped by graphene. *Opt. Quant. Electron.* **2017**, *49*, 163.
24. Bao, Q.; Chen, J.; Xiang, Y.; Zhang, K.; Li, S.; Jiang, X.; Xu, Q.H.; Loh, K.P.; Venkatesan, T. Graphene nanobubbles: A new optical nonlinear material. *Adv. Opt. Mater.* **2015**, *3*, 744–749.
25. Liu, J.; Park, S.; Nowak, D.; Tian, M.; Wu, Y.; Long, H.; Wang, K.; Wang, B.; Lu, P. Near-field characterization of graphene plasmons by photo-induced force microscopy. *Laser Photonics Rev.* **2018**, *12*, 1800040.
26. Meng, P.; Zhao, D.; Zhong, D.; Liu, W. Topological plasmonic modes in graphene-coated nanowire arrays. *Opt. Quant. Electron.* **2019**, *51*, 156.
27. Thongrattanasiri, S.; Silveiro, I.; Javier, G.d.A.F. Plasmons in electrostatically doped graphene. *Appl. Phys. Lett.* **2012**, *100*, 201105.
28. Jiang, L.; Guo, J.; Wu, L.; Dai, X.; Xiang, Y. Manipulating the optical bistability at terahertz frequency in the Fabry-Perot cavity with graphene. *Opt. Express* **2015**, *23*, 31181–31191.
29. Wang, F.; Qin, C.; Wang, B.; Long, H.; Wang, K.; Lu, P. Rabi oscillations of plasmonic supermodes in graphene multilayer arrays. *IEEE J. Sel. Top. Quant. Electron.* **2017**, *23*, 125–129.
30. Wang, Z.; Wang, B.; Long, H.; Wang, K.; Lu, P. Surface plasmonic lattice solitons in semi-infinite graphene sheet arrays. *J. Lightwave Technol.* **2017**, *35*, 2960–2965.
31. Chen, P.Y.; Alù, A. Atomically thin surface cloak using graphene monolayers. *ACS Nano* **2011**, *5*, 5855–5863.
32. Fang, Y.; Ouyang, Z. An approximately omnidirectional defect mode of the TE wave from one-dimensional photonic crystals doped by negative-index materials. *J. Opt. A Pure Appl. Opt.* **2009**, *11*, 045103.
33. Merano, M. Optical beam shifts in graphene and single-layer boron-nitride. *Opt. Lett.* **2016**, *41*, 5780–5783.
34. Zhai, C.; Zhang, Y.; Zhang, Q. Characterizing the ellipticity of an isolated attosecond pulse. *Opt. Commun.* **2019**, *437*, 104–109.
35. Wang, R.; Zhang, Q.; Li, D.; Xu, S.; Cao, P.; Zhou, Y.; Cao, W.; Lu, P. Identification of tunneling and multiphoton ionization in intermediate Keldysh parameter regime. *Opt. Express* **2019**, *27*, 6471–6482.
36. Xiang, Y.X.; Guo, J.; Dai, X.Y.; Wen, S.C.; Tang, D.Y. Engineered surface bloch waves in graphene-based hyperbolic metamaterials. *Opt. Express* **2014**, *22*, 3054–3062.

